Structural and luminescent properties of new Pb^{2+}-doped calcium chlorapatites $Ca_{10-x}Pb_x(PO_4)_6Cl_2$ ($0 \leq x \leq 10$)

2008 J. Phys.: Condens. Matter 20 275227

(http://iopscience.iop.org/0953-8984/20/27/275227)

J. Phys.: Condens. Matter **20** (2008) 275227 (6pp) doi:10.1088/0953-8984/20/27/275227

Structural and luminescent properties of new Pb^{2+}-doped calcium chlorapatites $Ca_{10-x}Pb_x(PO_4)_6Cl_2$ ($0 \leqslant x \leqslant 10$)

M Mehnaoui[1,2], R Ternane[2], G Panczer[1], M Trabelsi-Ayadi[2] and G Boulon[1]

[1] Laboratoire de Physico-Chimie des Matériaux Luminescents, UMR 5620, Université Claude Bernard Lyon 1, 69622 Villeurbanne, France
[2] Laboratoire d'Application de la Chimie aux Ressources et Substances Naturelles et à l'Environnement, Faculté des Sciences de Bizerte, 7021 Bizerte, Tunisie

E-mail: panczer@pcml.univ-lyon1.fr

Received 14 November 2007, in final form 17 March 2008
Published 6 June 2008
Online at stacks.iop.org/JPhysCM/20/275227

Abstract

Excitation and emission spectra of Pb^{2+} ions in $Ca_{10-x}Pb_x(PO_4)_6Cl_2$ ($0 \leqslant x \leqslant 10$) compounds are investigated for various activator concentrations at different temperatures. A calcium–lead chlorapatite system shows a common apatitic structure and occurs as a continuous solid solution. An attempt to identify the pure electronic transitions between the ground and the excited levels of Pb^{2+} is made. As a consequence of the two different sites in the apatite, two emission bands due to the $^3P_1 \rightarrow {}^1S_0$ (at room temperature) and $^3P_{0,1} \rightarrow {}^1S_0$ (at low temperature) transitions of the Pb^{2+} ions are observed. Decay times of Pb^{2+} emission have been measured. Experimental data point out thermalization between $^3P_1$ and $^3P_0$ levels, for example, at very low temperature, the forbidden transition $^3P_0 \rightarrow {}^1S_0$ is the most intense. The overlap between the emission band of one site and the excitation band of the other site corresponds to an energy transfer phenomenon. Correlations between the luminescence results and the structural data are discussed.

(Some figures in this article are in colour only in the electronic version)

1. Introduction

The luminescence of compounds containing metal ions with s^2 configuration [1, 2] like Tl^+, Bi^{3+} and Pb^{2+} can be used in x-ray imaging devices, low pressure lamps, and high-energy physics [3]. The optical properties of Pb^{2+} have been progressively studied as an activator or in the host matrix [4]. The luminescence properties of the Pb^{2+} ion with $6s^2$ configuration are attributed to the ground state $^1S_0$ and two excited states of singlet $^1P_1$ and triplet $^3P_{0,1,2}$ [5]. Usually, Pb^{2+} emission is located from the UV to visible range whereas Pb^{2+} absorption is located in the UV range only.

The crystal structure of apatite ($M_{10}(PO_4)X_2$, M being an alkaline rare earth and X being a halogen, oxygen, or hydroxyl ion) permits a wide range of cation and anion substitutions. Chlorapatite $Ca_{10}(PO_4)_6Cl_2$ crystallizes in the hexagonal system (space group $P6_3/m$), the cations are located on two non-equivalent sites. The site Ca (I), 4(f) position, with C_3 symmetry is coordinated by nine oxygens, whereas the site Ca(II), 6(h) position, is sevenfold coordinated (six oxygen and one Cl) with C_s symmetry [6].

Lead in apatite is of interest from two points of view. First, lead is known as a 'bone seeker' in that it accumulates in bones and teeth, second, this toxic heavy metal may contribute to deviations from the general formula of apatites. The substitution of calcium by lead in chlorapatites has been well studied; a preferential occupation of Pb^{2+} in the triangular Ca (II) sites has been shown [7–9].

In our laboratory, previous studies were devoted to the luminescence of some apatites doped with rare earth elements [10–13]. Interesting features were pointed out due to the presence of the two Ca I and Ca II substitution sites for the activator.

In this paper, we report the results of the structural characterization and for the first time the Pb^{2+} luminescent properties in $Ca_{10-x}Pb_x(PO_4)_6Cl_2$ ($0 \leqslant x \leqslant 10$) in order to enhance a possible application of these materials as near-ultraviolet or blue emitting phosphors.

2. Experimental details

2.1. Synthesis

Samples corresponding to $Ca_{10-x}Pb_x(PO_4)_6Cl_2$ ($0 \leqslant x \leqslant 10$) were prepared through the solid state reaction using starting materials $CaCO_3$, $CaCl_2{\cdot}2H_2O$, PbO, $PbCl_2$, and $(NH_4)_2HPO_4$ with defined proportions. The mixtures were pressed under 5–10 T cm^{-2}, the pellets were calcined at 500 °C for 24 h and then at 700 °C for 3 days. The heat treatment was performed in a platinum crucible with intermediate grindings in order to obtain a homogeneous mixture and completeness of the reaction. The formation of lead-substituted calcium chlorapatites can be described according to the following reactions:

For $x \geqslant 1$,

$$(10-x)CaCO_3 + (x-1)PbO + PbCl_2 + 6(NH_4)_2HPO_4 \rightarrow Ca_{10-x}Pb_x(PO_4)_6Cl_2 + (10-x)CO_2 + 12NH_3 + 9H_2O.$$

For $x \leqslant 1$

$$(9-x)CaCO_3 + CaCl_2{\cdot}2H_2O + xPbO + 6(NH_4)_2HPO_4 \rightarrow Ca_{10-x}Pb_x(PO_4)_6Cl_2 + (9-x)CO_2 + 12NH_3 + 11H_2O.$$

2.2. Characterization

2.2.1. Chemical analysis. The Ca, Pb, P, and Cl contents were determined by plasma emission spectroscopy (ICP).

2.2.2. X-ray powder diffraction (XRD). X-ray diffraction measurements were carried out at room temperature using a Siemens D8 diffractometer with Cu Kα radiation (λ = 1.5406 Å). The a and c lattice parameters were determined using the Checkcell software.

2.2.3. Infrared spectroscopy (IR). The infrared spectra were recorded on pellets using 1 mg of apatite powder in 300 mg of powdered spectroscopic grade KBr, with the Perkin Elmer model GX Fourier transform infrared (FTIR) spectrometer in the range of 4000–400 cm^{-1}.

2.2.4. Pb^{2+} luminescence. The luminescence spectra were measured under a Nd:YAG laser (Spectra Physics Quanta-Ray, GCR130) which delivers pulses of 10 ns duration and 0.1 cm^{-1} spectral width. The luminescence observed at the geometry of 45° was analyzed by a f-125 monochromator with a grating of 400 and 1200 grooves mm^{-1} and detected by an Instaspec ICCD detector enabling time-resolved spectra acquisition: delay times and gate pulse duration between 10 ns and 9 ms. The UV excitation spectra were recorded with a 450 W xenon lamp associated with a monochromator Gemini 180 from Jobin-Yvon. The life time analysis of the decay curves was accomplished by an Origin computer program.

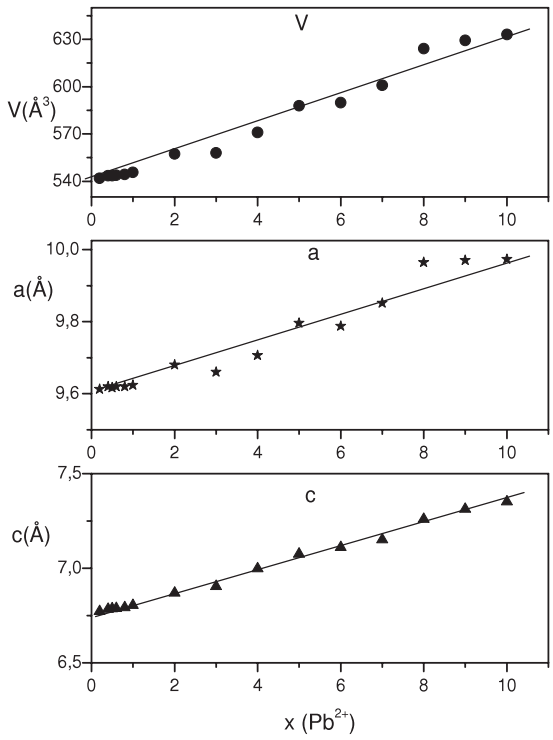

Figure 1. Variations of the cell parameters a, c and volume V of $Ca_{10-x}Pb_x(PO_4)_6Cl_2$ as a function of the lead content (x).

3. Results and discussion

3.1. X-ray analysis

The purity of the samples was controlled by x-ray diffraction. All the samples reveal the existence of one single phase indexed on the hexagonal $P6_3/m$ apatite structure. Figure 1 gives the evolution of the lattice parameters and the volume of $Ca_{10-x}Pb_x(PO_4)_6Cl_2$ compounds. The increase of these parameters is observed as x increases. This is in agreement with the substitution of the calcium with the lowest ionic radii ($r(Ca^{2+}) = 0.99$ Å [14]) by the lead ($r(Pb^{2+}) = 1.2$ Å [14]). The variation of the parameters is essentially linear and follows the Végard law [15]. This indicates a complete solubility and the formation of a continuous solid solution of calcium–lead chlorapatites.

3.2. Chemical analysis

The results of the chemical analysis of the 2% Pb^{2+}-doped $Ca_{10}(PO_4)_6Cl_2$ is reported in table 1. The experimental Ca, Pb, and P contents are slightly lower than the theoretical values. The recalculated formula from the average result of four analyses is $Ca_{9.32}Pb_{0.17}(PO_4)_{6.03}Cl_{1.92}$.

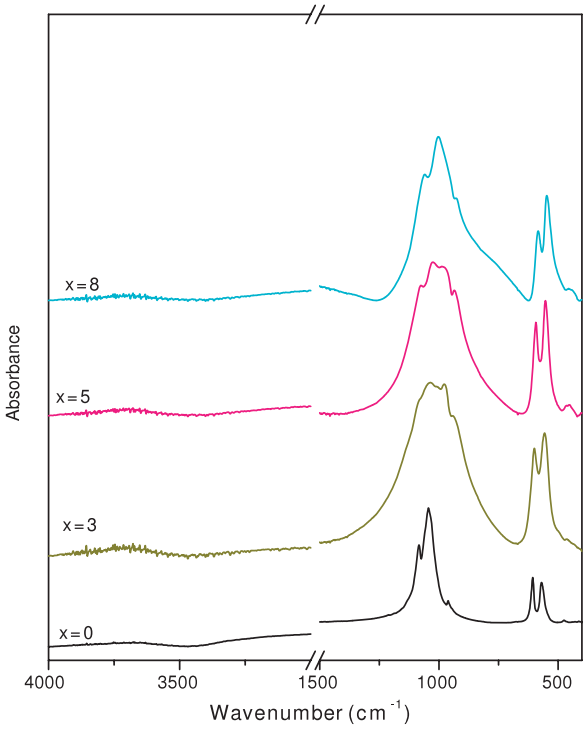

Figure 2. FTIR spectra of $Ca_{10-x}Pb_x(PO_4)_6Cl_2$.

Table 1. Chemical analysis of 2% Pb^{2+}-doped $Ca_{10}(PO_4)_6Cl_2$.

Element	wt (%) (theoretical)	wt (%) (experimental)
Ca	36.43	34.75
Pb	3.84	3.36
P	17.29	17.37
Cl	6.57	6.84
Formula	$Ca_{9.8}Pb_{0.2}(PO_4)_6Cl_2$	$Ca_{9.32}Pb_{0.17}(PO_4)_{6.03}Cl_{1.92}$

3.3. IR investigation

All the samples show that the IR absorption spectra is typical of chlorapatites (figure 2). The absence of the bands due to OH^- (633 cm^{-1}), CO_3^{2-} (1410–1450, 860–885 cm^{-1}), and HPO_4^{2-} (1180–1200, 875 cm^{-1}) ions indicates the absence of appreciable amounts of impurities [16, 17]. The IR spectra are dominated by two groups of bands. A first group of bands located between 522 and 606 cm^{-1} attributed to $\delta_{as}(PO_4)$ (antisymmetric deformation) in the apatitic structure. A second group of bands located at 1043–1087 cm^{-1} is attributed to the $\nu_{as}(PO_4)$ vibrations (antisymmetric elongation) in the apatitic structure. The shoulder situated at 402–474 cm^{-1} is assigned by the $\delta_s(PO_4)$ mode (symmetrical deformation) while the bands situated at 918–957 cm^{-1} are attributed to the $\nu_s(PO_4)$ (symmetrical elongation) in the apatitic structure. These bands shift progressively toward lower frequency with the increase of lead content (x) (figure 3). As reported by Hadrich *et al* for $Ca_{10-x}Pb_x(PO_4)_6(OH)_2$ compounds [18], the decrease of the frequencies of the PO_4 internal vibration modes reveals stronger Pb–O interactions in the sixfold site compared with the Ca–O ones which can be explained by partial covalent bonds [19]. This was observed in the crystal

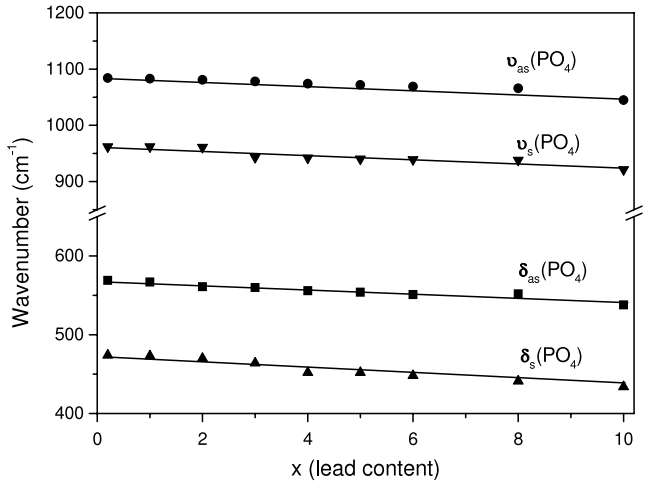

Figure 3. Variations of the IR frequencies of PO_4 group fundamental modes for $Ca_{10-x}Pb_x(PO_4)_6Cl_2$ as a function of the lead content (x).

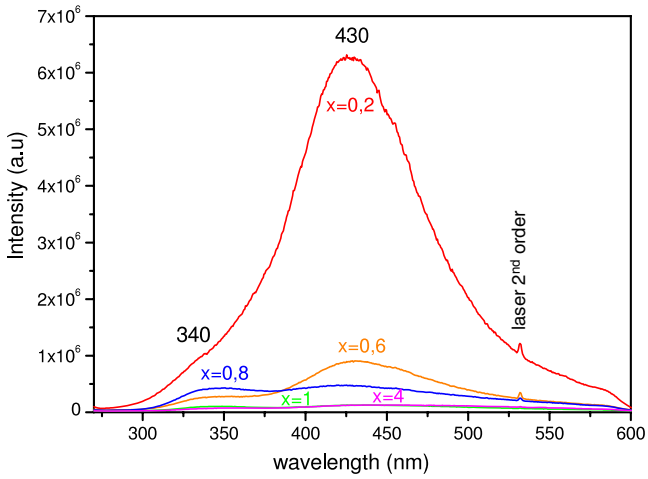

Figure 4. Concentration quenching of $Ca_{10-x}Pb_x(PO_4)_6Cl_2$ under 266 nm at 77 K.

structure of nasonite, $Pb_6Ca_4(Si_2O_7)_3Cl_2$ [20], which clearly shows partially covalent bonds between Pb and O, on the one hand, and between Pb and Cl, on the other. The structure of this compound is related to that of the apatite one, the Cl^- ions being situated in the channels. The broadening of the IR bands with increasing x is explained by the substitution effect.

3.4. Pb^{2+} luminescent properties

3.4.1. Emission spectra. The emission spectra were measured for different Pb^{2+} contents. At room temperature, the emission spectrum of 2% Pb^{2+}-doped $Ca_{10}(PO_4)_6Cl_2$ under 266 nm laser excitation shows one broad band with a maximum at about 340 nm and a second more intense one that can be observed at 430 nm (figure 4). These two bands observed are attributed to the $^3P_1 \rightarrow {}^1S_0$ allowed electronic transition of Pb^{2+} in the two Ca I and Ca II sites [21, 22]. From $x \geqslant 1$ (10%), we observed a high quenching of the blue emission (figure 4).

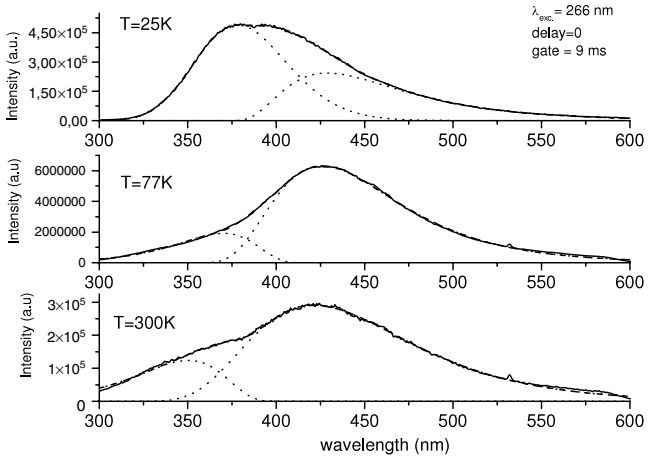

Figure 5. Pb^{2+} emission spectra of 2% Pb^{2+}-doped $Ca_{10}(PO_4)_6Cl_2$ under 266 nm laser excitation at different temperatures. Deconvolution curves with Gaussian profiles are shown by a dotted line. Result of the fit is shown by a dashed line.

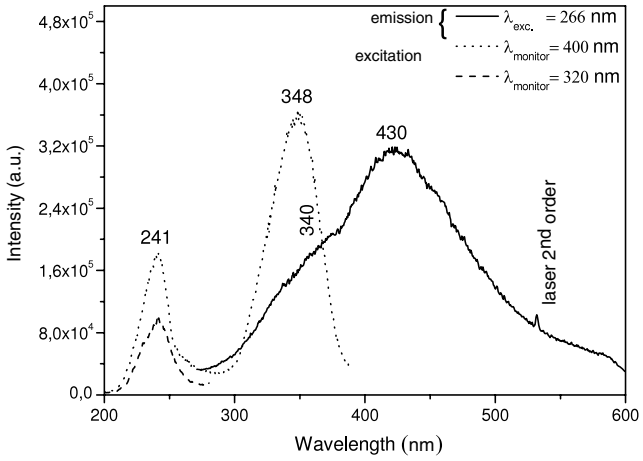

Figure 6. Excitation (dashed line) and emission (solid line) spectra of 2% Pb^{2+}-doped $Ca_{10}(PO_4)_6Cl_2$ at room temperature.

According to Andres-Verges *et al* [23] and to our recent results on the luminescence of divalent lead in the calcium hydroxyapatites [24], the blue intense emission is ascribed to Pb^{2+} ions in the Ca II site whereas the weak UV emission is related to Pb^{2+} ions in the Ca I site. As the temperature decreases the ultraviolet band becomes more intense us is usual in such compounds and shifts towards the higher wavelength as the deconvolution of the spectra shows it. The behavior already found for the emission spectrum of Bi^{3+}-doped oxides, with the occurrence of the $^3P_0$ level at lower energy than the $^3P_1$ one, is shifted to higher wavelengths [20] (figure 5).

3.4.2. Excitation spectra. The excitation spectra of 2% Pb^{2+}-doped $Ca_{10}(PO_4)_6Cl_2$ are shown in figure 6. Two main excitation bands with maxima at 241 and 348 nm are observed. The excitation spectrum monitored at $\lambda = 400$ nm shows two broad bands, the first one is positioned at 348 nm and attributed to the $^1S_0 \rightarrow {}^3P_1$ (A-band) transition of Pb^{2+} in the Ca II site, the second one is located at 241 nm. This band appears in the excitation spectrum monitored for $\lambda = 320$ nm, which shows this unique 241 nm band attributed to the $^1S_0 \rightarrow {}^3P_1$ transition of Pb^{2+} in the Ca I site. The overlap of the emission band at 340 nm and the excitation band at 348 nm (figure 5) reveals an energy transfer: the light emitted by Pb (Ca I) sites at 340 nm can be partially transferred by both nonradiative and radiative energy transfer to Pb (Ca II) sites which are emitting a blue emission band. It has to be noted that the Stokes is shift important between the excitation maxima and the $^3P_1 \rightarrow {}^1S_0$ emission. The Stokes shift amounts to 12 082 cm^{-1} and 4916 cm^{-1} for the ultraviolet and the visible emissions, respectively.

3.4.3. Luminescent lifetime. A useful property of phosphor activators is the decay rate of the corresponding radiative process, which is accessible to measurement and relevant to phosphor efficiency and to site symmetry of the activators.

Because of the important variations of the *lifetime* τ and of the theoretical interpretation according to the exponential of Boltzmann, the curves as $\log\tau = 1/T$ are presented. They are similar for all the phases and depend on the concentration. As a matter of fact, for the 2% Pb^{2+}-doped $Ca_{10}(PO_4)_6Cl_2$, the decay (figure 7) of the ultraviolet emission (340 nm) is longer than the blue one (430 nm). This is in agreement with the fact that the symmetry C_3 of the Pb I site (340 nm) is higher than the Cs symmetry of the Pb II one (430 nm).

Three principal parts are observed:

- $T < 40$ K. The lifetime reaches a limit value ranging between 800 μs at 20 K and 500 μs at 40 K for Pb^{2+} in the Ca I site whereas the decay times in the Ca II site range between 250 μs at 20 K to 100 μs at 40 K.
- $40 < T <$ 150–200 K. The lifetime τ of the ultraviolet emission decreases with an exponential law, the function $\log\tau = f(1/T)$ being linear. The observed overlap (figure 7) in the temperature range between 100 and 150 K shows that the levels' behavior is the same for the two sites.
- $T >$ 200 K. The lifetime τ decreases not exponentially but more quickly. It is the field of intervention of nonradiative transitions. Moreover, we notice that for some compounds, τ can be represented by the sum of two decays.

3.4.4. Discussion. From the obtained results, we consider the excitation process in which the transitions are provided from the $^3P_1$ level. It is also necessary to take into account the presence of the metastable level $^3P_0$ located just below $^3P_1$ [1].

Moreover, according to the site symmetry, the $^3P_1$ excited level can be split into two components in the C_3 site or three in the Cs site (table 2). It is thus necessary to interpret the kinetics with a system including at least four levels.

It has been assumed that the $^3P_0 \rightarrow {}^1S_0$ transition occurs in the mechanism of emission although the $^3P_0$ level is metastable. The $^1S_0 \rightarrow {}^3P_0$ absorption transition remains negligible in front of the $^1S_0 \rightarrow {}^3P_1$ one and we will suppose that only this last transition occurs in the excitation mechanism.

The separation of the maxima in wide bands for both the excitation and the emission spectra is made difficult by

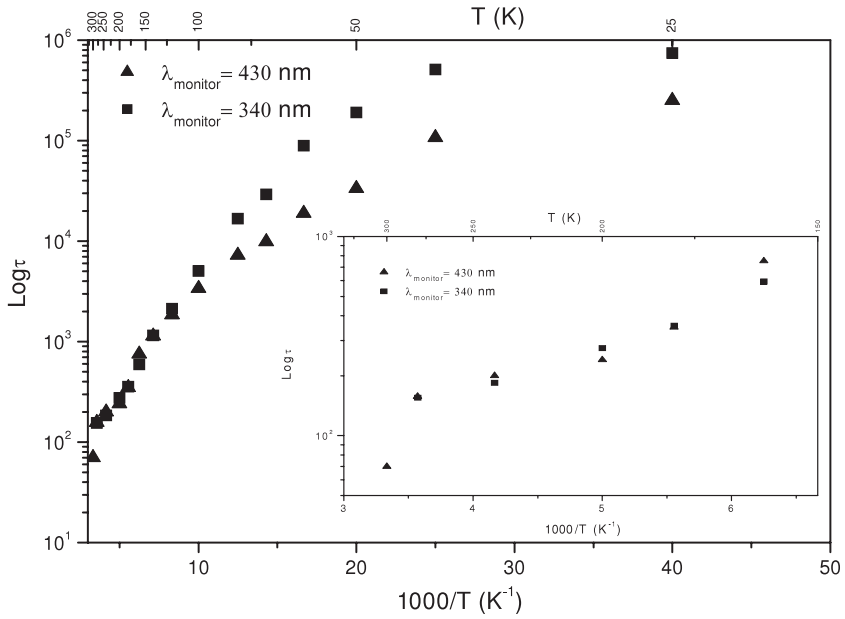

Figure 7. Temperature dependence of the decay time of 2% Pb^{2+}-doped $Ca_{10}(PO_4)_6Cl_2$ under 266 nm laser excitation.

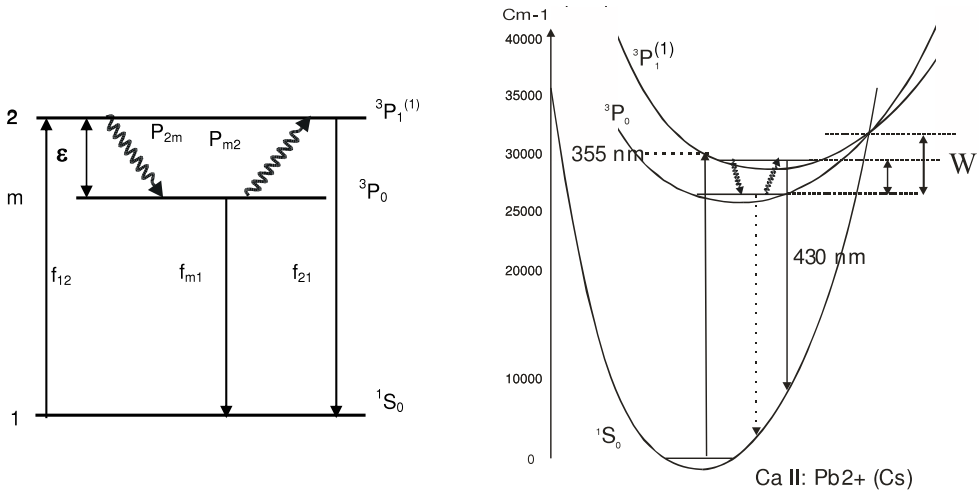

Figure 8. Pb^{2+} ion energy levels scheme in a system with three levels.

Table 2. Decomposition of the $^3P_1$ level with site symmetry of the apatite structure.

Site symmetry	Decomposition of the $^3P_1$ level
C_s	$2A'' + A'$
C_3	$A + E$

the weakness of the energy barrier (ε) and of the thermal activation energy (W) giving an idea of the thermal losses in the compounds. For the Pb^{2+} blue emission in the site Ca II (Cs), ε and W were estimated to be weak at about 75 and 200 cm^{-1}, respectively. In addition, for the usual $^3P_1 \rightarrow {}^1S_0$ emission, we studied only the lines originating from the first $^3P_1^{(1)}$ level, giving rise to the lower energy component. Thus, we have been interested only in the intense blue emission at room temperature and we simplified the model to explain the kinetics using a single system with three levels in which one is metastable, as shown in figure 8.

Let us consider the system on three levels in which (1) is the fundamental level ($^1S_0$), (2) is the excited level ($^3P_1$) and (m) is the metastable one ($^3P_0$). The $1 \rightarrow$ m transition being forbidden to all the electric and magnetic multipolar orders, the center can be excited only by $1 \rightarrow 2$ absorption of probability f_{12}. It can then turn over at the fundamental state either directly with radiative emission probability f_{21}, or via the intermediate of the metastable level m. During this process, as the metastable level is populated, the emission may occur by the m $\rightarrow$ 1 transition with probability f_{m1} much weaker than f_{21}. This diagram implies a decomposition of the emission spectra in two sub-bands, for example, the $2 \rightarrow 1$ energy should be higher than the m $\rightarrow$ 1 energy. Figure 5 shows clearly the expected UV and blue band shifts to smaller energy and then to higher wavelengths, when temperature

decreases from 300 to 25 K. At high temperature, under excitation in the $^3P_1$ level, a direct settling can occur to the $^1S_0$ fundamental level or another settling from the $^3P_0$ metastable level, involving the nonradiative transition $^3P_1^{(1)} \rightarrow {}^3P_0$ with P_{2m} probability. The emission can then occur in two ways.

- It can be either directly by the $^3P_0 \rightarrow {}^1S_0$ transition of which the f_{m1} probability is much weaker than that of transition $^3P_1^{(1)} \rightarrow {}^1S_0$ because of the forbidden transition ($\Delta J = 0$). So until roughly 40 K, the emission originates from the $^3P_0$ level.
- Or it can be by the $^3P_0 \rightarrow {}^3P_1^{(1)}$ rising with the probability P_{m2} with $P_{m2} = P_{2m} \exp(-\varepsilon/kT)$ when there is thermal equilibrium and so, in the $40 < T < 200$ K temperature range, both levels $^3P_0$ and $^3P_1^{(1)}$ can emit.

At higher temperature, the $^3P_1$ level is thermally populated, and, due to mixing of $^1P_1$ and $^3P_1$ states, the spin selection rule is partially lifted and the decay time of this allowed $^3P_1^{(1)} \rightarrow {}^1S_0$ emission is shortened.

4. Conclusion

The luminescence of Pb^{2+}-doped calcium chlorapatites originates from two kinds of sites. This is the consequence of the presence of two crystallographic sites in the apatite structure. At room temperature the two broad emission bands are assigned to two $^3P_1 \rightarrow {}^1S_0$ transitions whereas at low temperature they are interpreted by the thermal equilibrium between $^3P_1$ and the metastable $^3P_0$ states. Moreover, the superposition of the emission and excitation bands is connected with an energy transfer phenomenon in these compounds. Measurements of the luminescent lifetime under several excitations in the temperature range 20–300 K are in agreement with the emission from the $^3P_1$ and $^3P_0$ excited states.

To explain the strong dependence of the lifetime τ on temperature, the assumption of the metastable level $^3P_0$ is clearly demonstrated.

Experimental results show the possibility of using Pb^{2+} ion luminescent properties to detect very low lead content under UV excitation in synthetic and natural apatitic matrixes. Also, the intense emission at 430 nm could be potentially used in apatites as a blue emitting phosphor.

References

[1] Boulon G 1971 *J. Physique* **32** 333
[2] Blasse G and Dirksen G J 1985 *Mater. Chem. Phys.* **551–556** 12
[3] Folkerts H F, Zuidema J and Blasse G 1996 *Solid State Commun.* **99** 655
[4] Yun S J, Kim Y S and Park S H K 2001 *Appl. Phys. Lett.* **78** 721
[5] Blasse G 1998 *Prog. Solid State Chem.* **18** 79
[6] Elliott J C 1994 *Structure and Chemistry of the Apatites and Other Calcium Orthophosphates* (Amsterdam: Elsevier)
[7] Miyake M, Ishigaki K and Suzuki T 1986 *J. Solid State Chem.* **61** 230
[8] Mackie P E, Elliot J C and Young R A 1972 *Acta Crystallogr.* B **28** 1840
[9] Kim J Y, Ronald R and Kennedy B J 2000 *Aust. J. Chem.* **53** 679
[10] Ternane R, Trabelsi-Ayedi M, Kbir-Ariguib N and Piriou B 1999 *J. Lumin.* **81** 165
[11] Ternane R, Panczer G, Cohen-Adad M Th, Goutaudier C, Boulon G, Kbir-Ariguib N and Trabelsi-Ayedi M 2001 *Opt. Mater.* **16** 291
[12] Ternane R, Cohen-Adad M Th, Panczer G, Goutaudier C, Dujardin C, Boulon G, Kbir-Ariguib N and Trabelsi-Ayedi M 2002 *Solid State Sci.* **4** 53
[13] Ternane R, Boulon G, Guyot Y, Cohen-Adad M T, Trabelsi-Ayedi M and Kbir-Ariguib N 2003 *Opt. Mater.* **22** 117
[14] Shannon R D 1976 *Acta Crystallogr.* A **32** 751
[15] Végard L 1922 *Z. Phyzik.* **9** 395
[16] Ntahomvukiye I, Khattech I and Jemal M 1995 *Ann. Chim. Fr.* **1** 20
[17] Arends J, Christoffersen J, Christoffersen M R, Eckert H, Fowler B O, Heughebaert J C, Nancollas G H, Yesinowski J P and Zawacki S J 1987 *J. Cryst. Growth* **84** 515
[18] Hadrich A, Lautié A and Mhiri T 2001 *Spectrochim. Acta* A **57** 1673
[19] Piro O E, Apella M C, Baran E J and Rivero B E 1982 *Rev. Chim. Mineral.* **19** 11
[20] Giuseppetti G, Rossi G and Tadini C 1971 *Am. Mineral.* **56** 1174
[21] Boulon G, Pedrini C, Janin J and Curie D 1967 *Rev. Opt.* **46** 12
[22] Blasse G, Braam A W M and Heerschop M 1977 *J. Solid State Chem.* **20** 63
[23] Andres-Verges M, Higes-Rolando F J, Valenzuela-Calahorro C and Gonzales-Diaz P F 1983 *Spectrochim. Acta* A **39** 1077
[24] Mehnaoui M, Panczer G, Ternane R, Trabelsi-Ayedi M and Boulon G 2008 *Opt. Mater.* at press doi:10.1016/j.optmat.2007.11.006